



Walter+Eliza Hall  
Institute of Medical Research

Institute Research Publication Repository

***This is the author accepted version of :***

Sheikh BN, Phipson B, El-Saafin F, Vanyai HK, Downer NL, Bird MJ, Kueh AJ, May RE, Smyth GK, Voss AK, Thomas T. MOZ (MYST3, KAT6A) inhibits senescence via the INK4A-ARF pathway. *Oncogene*. 2015 34(37):5807-5820.

***which has been published in final form at***

doi: [10.1038/onc.2015.33](https://doi.org/10.1038/onc.2015.33);

## **MOZ (MYST3, KAT6A) inhibits senescence via the INK4A-ARF pathway**

Bilal N. Sheikh<sup>1,3</sup>, Belinda Phipson<sup>2,4</sup>, Hannah K. Vanyai<sup>1,3</sup>, Natalie L. Downer<sup>1</sup>, Farrah El-Saafin<sup>1,3</sup>, Matthew J. Bird<sup>4,5</sup>, Gordon K. Smyth<sup>2,6</sup>, Anne K. Voss<sup>1,3,7</sup>, and Tim Thomas<sup>1,3,7</sup>

<sup>1</sup> *Division of Development and Cancer, The Walter and Eliza Hall Institute of Medical Research, Melbourne 3052, Victoria, Australia*

<sup>2</sup> *Division of Bioinformatics, The Walter and Eliza Hall Institute of Medical Research, Melbourne 3052, Victoria, Australia*

<sup>3</sup> *Department of Medical Biology, University of Melbourne, Melbourne 3010, Victoria, Australia*

<sup>4</sup> *Murdoch Children's Research Institute, Flemington Rd., Melbourne 3052, Victoria, Australia*

<sup>5</sup> *Department of Paediatrics, University of Melbourne, Melbourne 3010, Victoria, Australia*

<sup>6</sup> *Department of Mathematics and Statistics, University of Melbourne, Melbourne 3010, Victoria, Australia*

<sup>7</sup> *These authors co-supervised this project and contributed equally*

Conflict of Interest: The authors declare no conflict of interest.

---

Running title: MOZ inhibits senescence via the INK4A-ARF pathway

Corresponding authors:

Tim Thomas, 1G Royal Parade, Melbourne 3052, Victoria, Australia, e-mail: [tthomas@wehi.edu.au](mailto:tthomas@wehi.edu.au) Ph: +61 3 93452477 Fax: +61 3 9347 0852

Anne K. Voss, 1G Royal Parade, Melbourne 3052, Victoria, Australia, e-mail: [avoss@wehi.edu.au](mailto:avoss@wehi.edu.au) Ph: +61 3 93452642 Fax: +61 3 9347 0852

Key words: MYST, epigenetics, ageing, CDC6, *Cdkn2a*

## Abstract

Cellular senescence is an important mechanism that restricts tumour growth. The *Ink4a-Arf* locus (also known as *Cdkn2a*), which encodes p16<sup>INK4A</sup> and p19<sup>ARF</sup>, plays a central role in inducing and maintaining senescence. Given the importance of cellular senescence in restraining tumour growth, great emphasis is being placed on the identification of novel factors that can modulate senescence. In this study, we show that the MYST-family histone acetyltransferase MOZ (MYST3/ KAT6A), first identified in recurrent translocations in acute myeloid leukaemia, is a potent inhibitor of senescence via the INK4A-ARF pathway. Primary mouse embryonic fibroblasts (MEFs) isolated from *Moz*-deficient embryos exhibit premature senescence, which was rescued on the *Ink4a-Arf*<sup>-/-</sup> background. Importantly, senescence resulting from the absence of MOZ was not accompanied by DNA damage, suggesting that MOZ acts independently of the DNA damage response. Consistent with the importance of senescence in cancer, expression profiling revealed that genes over-expressed in aggressive and highly proliferative cancers are expressed at low levels in *Moz*-deficient MEFs. We show that MOZ is required to maintain normal levels of histone 3 lysine 9 (H3K9) acetylation at the transcriptional start sites of at least four genes, *Cdc6*, *Ezh2*, *E2f2* and *Melk*, and normal mRNA levels of these genes. CDC6, EZH2 and E2F2 are known inhibitors of the INK4A-ARF pathway. This work establishes that MOZ is an upstream inhibitor of the INK4A-ARF pathway, and suggests that inhibiting MOZ may be one way to induce senescence in proliferative tumour cells.

## Introduction

The monocytic leukaemia zinc finger protein (MOZ) is a MYST family histone acetyltransferase (HAT), which was first identified in a recurrent translocation, t(8;16)(p11;p13) leading to an aggressive type of acute myeloid leukaemia (AML)<sup>1</sup>. Patients with a t(8;16) translocation, which generates a fusion transcript between MOZ and CBP, are typically diagnosed with a FAB M4/M5 sub-type of AML, commonly associated with coagulopathy, erythrophagocytosis and extramedullary dissemination<sup>2</sup>.<sup>3</sup> The prognosis of patients with a t(8;16) translocation is poor with median survival times, after diagnosis, reported between 2 months<sup>2</sup> and 4.7 months<sup>4</sup>. Gene expression analysis shows that this forms a distinct sub-type of AML that is typified by up regulation of HOX genes and their co-factor MEIS1<sup>4,5</sup>. Additional chromosomal

rearrangements have been identified that generate chimeric genes in which MOZ is fused to genes coding for other transcriptional regulators: NCOA2 (TIF2), NCOA3 and p300<sup>6-8</sup>. Consistent with the importance of self-renewal in leukemias, MOZ-TIF2 is able to induce the property of self-renewal in committed progenitors<sup>9</sup>.

Typically for an oncogene involved in haematological malignancy, studies of the normal function of MOZ show that it has an important role in normal haematopoiesis. Studies of loss-of-function mutations in MOZ have shown that it is essential for the development of hematopoietic stem cells<sup>10,11</sup>, and the HAT activity of MOZ is required for maintaining the self-renewal of HSCs<sup>12</sup>. During embryonic development, MOZ is required for the acetylation of histone 3 at lysine 9 (H3K9ac) at *Hox*<sup>13</sup>, *Tbx1* and *Tbx5* loci<sup>14</sup>, and for their correct expression. Accordingly, embryos lacking *Moz* show an extensive anterior homeotic transformation of the axial skeleton and neural tube<sup>13</sup>, as well as cardiac and craniofacial defects mirroring the human DiGeorge syndrome<sup>14</sup>.

Recent studies have examined the role of MOZ in cellular senescence. It has been reported that overexpressed MOZ is able to bind to p53, and that MOZ is required to activate *p21* expression in response to DNA damage to induce senescence<sup>15</sup>. This study suggests that in the absence of *Moz*, cells are unable to senesce and undergo apoptosis instead. However, a conflicting report has recently been published in which studies using mice that possess a catalytically inactive MOZ, suggest that the HAT activity of MOZ is important for restraining senescence<sup>16</sup>. It is unclear how the fundamental differences between these studies can be reconciled.

In order to examine the role of MOZ in senescence, we used primary MEFs isolated from *Moz*<sup>-/-</sup> embryos to show that endogenous MOZ is an inhibitor, and not an activator of senescence. Primary MEFs lacking MOZ undergo premature senescence at passage 3 and express the senescence markers  $\beta$ -galactosidase, *Ink4a* and *Arf*. Apoptotic cell death was unaffected in *Moz*<sup>-/-</sup> cultures. Using microarray and chromatin immunoprecipitation (ChIP), we show that MOZ is required for the maintenance of H3K9ac at gene loci encoding repressors of the INK4A-ARF pathway including *Cdc6*, *Ezh2* and *E2f2*. Consistent with these findings, we show that premature senescence in *Moz*-deficient cells was rescued completely by deletion of the *Ink4a-Arf* locus. This work identifies MOZ as an upstream inhibitor of the INK4A-ARF pathway and premature senescence.

## Results

### Primary *Moz*-deficient MEFs show premature senescence

To investigate the role of MOZ in cellular senescence, we isolated and cultured primary fibroblasts from E12.5 wild type, *Moz*<sup>+/-</sup> and *Moz*<sup>-/-</sup> embryos. Compared to wild type, *Moz*<sup>-/-</sup> cultures failed to accumulate cells from passage three onwards (Figure 1a;  $p < 0.001$ ,  $n = 4$  *Moz*<sup>+/+</sup>, 5 *Moz*<sup>-/-</sup> cultures). *Moz*<sup>+/-</sup> MEFs showed an intermediate phenotype, with a failure to accumulate cells from passage six onwards. These data indicated that *Moz*-deficient MEFs were either defective in cell proliferation, exhibited increased cell death, or underwent cellular senescence prematurely.

A senescent phenotype is characterised by an increase in  $\beta$ -galactosidase activity<sup>17</sup>, increased reactive oxygen species (ROS) production<sup>18</sup>, and an increase in the levels of senescence inducers p16<sup>INK4A</sup> and p19<sup>ARF</sup>. We compared these parameters of cellular senescence in wild type and *Moz* mutant MEFs.  $\beta$ -galactosidase activity was increased in *Moz*<sup>-/-</sup> cultures from passage two onwards (Figure 1b,c). At passage two, a 50% increase in  $\beta$ -galactosidase activity was observed in *Moz*<sup>-/-</sup> cultures ( $p = 0.005$ ), while the levels of  $\beta$ -galactosidase activity were more than two-fold higher in *Moz*<sup>-/-</sup> cultures from passage 3 onwards (Figure 1c, Figure S1,  $p < 0.001$ ,  $n = 5$  wild type, 3 *Moz*<sup>-/-</sup> cultures). Consistent with the proliferation characteristics of *Moz*<sup>+/-</sup> cells, there was significantly more  $\beta$ -galactosidase activity in *Moz*<sup>+/-</sup> cultures from passage 4 onwards compared to wild type cultures ( $p < 0.01$ ,  $n = 4$  *Moz*<sup>+/+</sup> cultures). Consistent with the reported increase in ROS in senescent cells<sup>18</sup>, a 70% increase in ROS production ( $O_2\bullet$ ) was observed in *Moz*<sup>-/-</sup> cultures at passage three compared to wild type (Figure 1d,  $p < 0.001$ ,  $n = 6$  *Moz*<sup>+/+</sup>, 11 *Moz*<sup>-/-</sup> cultures). We compared *Ink4a*, *Arf* and *Ink4b* mRNA levels at passage five between wild type and *Moz*<sup>-/-</sup> cultures (Figure 1e). Compared to wild type, a 13-fold increase in *Ink4a* levels ( $p = 0.031$ ), a 2.6-fold increase in *Arf* levels ( $p = 0.012$ ), and a 1.8-fold increase in *Ink4b* mRNA levels ( $p = 0.002$ ) were observed in *Moz*<sup>-/-</sup> cultures ( $n = 3$ ). Altogether, the increase in (1)  $\beta$ -galactosidase activity, (2) increased ROS production, and (3) an increase in *Ink4a*, *Arf* and *Ink4b* mRNA all suggest that *Moz*-deficient MEFs fail to proliferate due to premature senescence.

### Proliferation in *Moz*<sup>-/-</sup> MEFs is only affected at late passages

Since senescence results in cell cycle arrest, we tested whether DNA synthesis was affected in *Moz*-deficient cultures by examining incorporation of the thymidine analogue BrdU and analysing cell cycle characteristics. At passage two, there was no

difference in BrdU incorporation between wild type and *Moz*<sup>-/-</sup> MEFs, suggesting that DNA synthesis and cell proliferation was relatively normal at this time point (Figure 1f,  $p = 0.231$ ,  $n = 4$  wild type, 5 *Moz*<sup>-/-</sup> cultures). At passage four, 2.2-fold fewer *Moz*<sup>-/-</sup> MEFs stained positive for BrdU compared to wild type cultures ( $p = 0.05$ ). These data were consistent with the cell cycle profiles of MEF cultures assayed by Ki67 and DAPI staining, and analysed by flow cytometry (Figure S2). Together, these data suggest that proliferation is not a primary defect in early-passage *Moz*-deficient MEFs. Rather, the reduced proliferation in *Moz*<sup>-/-</sup> cells at later passages likely reflects increased senescence.

### **Apoptosis is not affected in MEFs lacking MOZ**

It has been previously suggested that in response to UV or drug-induced DNA damage, *Moz*<sup>-/-</sup> MEFs undergo apoptosis at an increased rate compared to wild type<sup>15</sup>. Therefore, we tested whether the failure of cell accumulation in primary *Moz*<sup>+/-</sup> and *Moz*<sup>-/-</sup> MEF cultures might be due to an increase in cell death. The proportion of apoptotic cells in wild type ( $n = 5$ ), *Moz*<sup>+/-</sup> ( $n = 4$ ) and *Moz*<sup>-/-</sup> ( $n = 3$ ) cultures was determined over 72 hours after passages two, four and six by annexin V binding of externalised phosphatidylserine (Figure 1g). Compared to wild type, there was no difference in the proportion of annexin V-binding cells in *Moz*<sup>+/-</sup> cultures at all time points analysed ( $p > 0.10$ ). Similarly, the proportion of annexin V-binding cells in *Moz*<sup>-/-</sup> was similar to wild type, apart from a small increase of approximately 2% in annexin V-binding cells 48 hours after passages two and four. These data show that apoptotic cell death is not the major cause of the failure of cell accumulation in *Moz*<sup>+/-</sup> and *Moz*<sup>-/-</sup> primary MEF cultures.

### **Premature senescence in *Moz*-deficient cultures is independent of DNA damage**

A major cause of cellular senescence is DNA damage<sup>19</sup>. Since MEFs deficient in repairing double stranded DNA breaks senesce prematurely<sup>19</sup>, and previous work has suggested that *Moz*-deficient MEFs are unable to senesce in response to DNA-damage<sup>15</sup>, we determined whether *Moz*-deficient MEFs had an increased level of DNA damage. In response to double stranded breaks, histone H2A.X is phosphorylated at serine-139 (Figure 2a,  $\gamma$ H2A.X)<sup>20</sup>, and this modification can be detected by flow cytometry<sup>21</sup>. *Moz* MEFs were separated based on the quantity of DNA, to ensure that

the levels of  $\gamma$ H2A.X staining were determined proportionally to the amount of DNA in the cell (Figure S3). Levels of  $\gamma$ H2A.X staining increased with passage number (Figure 2b). This is consistent with the reported increased senescence in MEFs over multiple passages<sup>19</sup>. The levels of  $\gamma$ H2A.X staining of wild type (n = 5), *Moz*<sup>+/-</sup> (n = 4), and *Moz*<sup>-/-</sup> cultures (n = 3) were similar at passages one and five. At passage three, there was a small but significant increase in  $\gamma$ H2A.X levels in *Moz*<sup>-/-</sup> MEFs compared to wild type ( $p < 0.01$ ). However, this small increase in  $\gamma$ H2A.X levels in *Moz*<sup>-/-</sup> MEFs at passage three is unlikely to explain the continuous increase in senescence observed as early as passage two in *Moz*<sup>-/-</sup> MEFs (Figure 1c).

### **The premature senescence phenotype in *Moz*-deficient MEFs is also present at physiological levels of oxygen (3% O<sub>2</sub>)**

MEFs cultured at physiological oxygen levels (3%) accumulate significantly less DNA damage and are therefore able to avoid early senescence<sup>19</sup>. To determine if the premature senescence phenotype observed in *Moz*-deficient MEFs was evident at physiological tissue levels of oxygen, we analysed the growth characteristics of MEFs grown at 3% O<sub>2</sub>. Over the first five passages, there were no differences in the number of cells in wild type (n = 6), *Moz*<sup>+/-</sup> (n = 5) and *Moz*<sup>-/-</sup> (n = 5) cultures (Figure 2c,  $p > 0.05$ ). From passage 6 onwards, there were significantly fewer cells in *Moz*<sup>-/-</sup> cultures compared to wild type ( $p < 0.05$ ). Similarly, from passage 8 onwards, there were significantly fewer cells in *Moz*<sup>+/-</sup> cultures compared to wild type ( $p < 0.05$ ). To confirm that the decrease in cells in *Moz*<sup>-/-</sup> cultures was due to increased senescence, we analysed the expression levels of the senescence markers and inducers *Ink4a*, *Arf* and *Ink4b*. We chose to analyse passage five MEFs as this was before the decrease in *Moz*<sup>-/-</sup> MEFs was first evident. At passage five, mRNA levels of *Ink4a* were increased 2.9-fold ( $p < 0.001$ ), *Arf* 1.73-fold ( $p = 0.001$ ), and *Ink4b* 2-fold in *Moz*<sup>-/-</sup> cultures ( $p = 0.001$ , Figure 2d, n = 4 wild type and 4 *Moz*<sup>-/-</sup> cultures). These data suggest that *Moz*<sup>-/-</sup> MEFs also show premature senescence, albeit delayed, when cultured in 3% O<sub>2</sub>. Thus, increased senescence in *Moz*-deficient MEFs is unlikely to be related to increased DNA damage.

To ensure that the primary defect was not related to cell proliferation or apoptosis at 3% oxygen, we analysed cell proliferation and cell death. At passages two and five, there

was a reduction in BrdU incorporation in *Moz*<sup>-/-</sup> MEFs compared to wild type (Figure 2e,  $p < 0.05$ ,  $n = 4$  wild type, 5 *Moz*<sup>-/-</sup>). However, cell cycle parameters analysed by Ki67 staining and DAPI were normal at passage two, and only revealed a decrease in *Moz*-deficient cells in the G2/M-phase at passages five and eight (Figure S4,  $p < 0.05$ ). The rate of apoptotic cell death in each culture was determined by annexin V staining. We analysed the proportion of apoptotic cells in wild type ( $n = 4$ ), *Moz*<sup>+/-</sup> ( $n = 3$ ) and *Moz*<sup>-/-</sup> ( $n = 5$ ) cultures over 72 hours after passages two, five and seven. There were no significant differences between any of the genotypes at all nine time points analysed (Figure 2f). Thus, consistent with our results at atmospheric (20%) oxygen, the reduction in *Moz*<sup>-/-</sup> MEFs at physiological oxygen levels (3%) was primarily due to early senescence.

### Expression profile of *Moz*-deficient MEFs

To identify genes regulated by MOZ in MEFs, we carried out microarray analysis using RNA isolated from passage 3 wild type, *Moz*<sup>+/-</sup> and *Moz*<sup>-/-</sup> (Figure 3a). We used passage 3 MEFs as senescence levels in *Moz*<sup>+/-</sup> cultures were the same as wild type, while *Moz*<sup>-/-</sup> cultures showed a mild increase in senescence at passage 3 compared to later passages (Figure 1). Using a false discovery rate (FDR) cut-off of 10% (equivalent to  $p < 0.0015$ ), we found 205 genes to be differentially expressed in *Moz*<sup>-/-</sup> cultures compared to wild type (Figure 3b, Table S1), and only three genes to be differentially expressed in *Moz*<sup>+/-</sup> cultures compared to wild type (Table S2). Since *Moz*<sup>+/-</sup> MEFs have an intermediate phenotype compared to wild type and *Moz*<sup>-/-</sup> cultures (Figure 1), we combined the information from *Moz*<sup>+/-</sup> and *Moz*<sup>-/-</sup> cultures to look for genes that show a graduated change in expression from wild-type to *Moz*<sup>+/-</sup> to *Moz*<sup>-/-</sup> fibroblasts. This allowed us to identify 269 genes that were differentially expressed in the *Moz*-deficient cultures (Table S3). The combined analysis provided increased statistical power, so we used this gene list for all subsequent analysis.

We investigated whether genes differentially expressed in *Moz* mutant cultures correlated with published senescence, proliferation and apoptosis datasets. Mutations in the gene encoding the pre-laminin A processing enzyme *Zmpste24* lead to premature ageing, and consistently, *Zmpste24*<sup>-/-</sup> MEFs show premature senescence<sup>22</sup>. Interestingly, there was a strong overlap between the *Moz* dataset and the *Zmpste24*<sup>-/-</sup> MEF dataset (Figure 3c). Genes up-regulated in *Zmpste24*<sup>-/-</sup> MEFs were also over-expressed in *Moz*-

deficient cultures ( $p = 0.021$ ), while genes down-regulated in *Zmpste24*<sup>-/-</sup> MEFs were also reduced in *Moz*-deficient MEFs ( $p = 0.009$ ). Furthermore, targets of p53 that are down-regulated during senescence<sup>23</sup> were over-represented in *Moz* wild type MEFs ( $p = 0.05$ ). In contrast, there was no overlap between genes differentially expressed in oncogene (RASV12)-induced senescence<sup>24</sup> and the *Moz* dataset ( $p > 0.90$ ). Consistent with the senescence phenotype in *Moz*<sup>-/-</sup> MEFs, genes associated with proliferation in both aggressive undifferentiated cancers<sup>25</sup> and in liver cancer (Hepatocellular carcinoma)<sup>26</sup>, were more highly expressed in wild type and not *Moz*-mutant MEFs (Figure 3d,  $p < 0.05$ ). In contrast to senescence and proliferation related genes, no correlation was observed between apoptosis-related genes and the *Moz* dataset (Figure 3e,  $p > 0.25$ ). We also compared the *Moz* dataset to datasets available through the Broad Institute. The top 30 datasets best correlating with the *Moz* dataset are provided in Figure 3f, while the complete list can be found in Table S4. These comparisons show that genes that are normally over-expressed in cancers, particularly aggressive cancers, were under-expressed in *Moz*-deficient cultures compared to wild type MEFs. Altogether, these analyses suggest that decreased levels of MOZ lead to a gene-expression profile associated with increased senescence and decreased cell proliferation.

### **The premature senescence of *Moz*<sup>-/-</sup> MEFs is rescued by deletion of *Ink4a-Arf***

Our phenotypic and expression analyses both suggested that *Moz*<sup>-/-</sup> MEFs senesce prematurely. Cell cycle progression is regulated by cyclins and cyclin-dependent kinases (CDKs), which advance cells through phases of the cell cycle. Senescence is generally induced and maintained by proteins that inhibit the cyclin-CDK complexes<sup>27-29</sup>. There are two families of CDK inhibitors, namely the INK4 and CIP-KIP families<sup>27-29</sup>. The INK4 family consists of INK4A, INK4B, INK4C and INK4D, while the CIP-KIP family consists of p21<sup>CIP1</sup>, p27<sup>KIP1</sup> and p57<sup>KIP2</sup>. To determine whether any CDK inhibitors are affected by the absence of MOZ, we quantified the mRNA levels for these families in sub-confluent MEFs, one day after passage three.

Compared to wild type, there was a 2.6-fold increase in *Ink4a* mRNA (Figure 4a,  $p = 0.001$ ,  $n = 4$  wild type and *Moz*<sup>-/-</sup>) and a 1.9-fold increase in *Arf* mRNA in *Moz*<sup>-/-</sup> MEFs ( $p = 0.022$ ). Similarly, *Ink4b*, which lies adjacent to the *Ink4a-Arf* locus, showed a 2.2-fold increase in mRNA in *Moz*<sup>-/-</sup> MEFs ( $p = 0.005$ ). In contrast, *Ink4c* ( $p = 0.003$ ) and

*Ink4d* ( $p = 0.042$ ) showed a small but significant decrease at the mRNA level in *Moz*<sup>-/-</sup> MEFs. The *CIP-KIP* family members showed comparably minor changes (Figure 4b). Compared to wild type, there was a small but significant increase in the level of *p21* mRNA ( $p = 0.042$ ), while *p27* ( $p = 0.104$ ) and *p57* ( $p = 0.089$ ) levels were unchanged. At the protein level, increased levels of p16<sup>INK4A</sup> and p19<sup>ARF</sup>, but not p21<sup>CIP1</sup>, were observed in passage 3 *Moz*<sup>-/-</sup> MEFs (Figure S5). Together, these data imply that increased expression of the *Ink4a-Arf* and the adjacent *Ink4b* locus is the most likely cause of premature senescence in *Moz*<sup>-/-</sup> MEFs. These data are consistent with the increase in *Ink4a* and *Arf* mRNA levels in passage 5 MEFs (Figure 1e), and the microarray data, which showed an increase in *Ink4a* and *Arf* (*Cdkn2a*) mRNA expression (Table S1).

Previous work has shown that MEFs lacking *Ink4a-Arf* escape cellular senescence<sup>30</sup>. Therefore, we hypothesized that if MOZ regulated senescence through the INK4A-ARF pathway, ablating *Ink4a-Arf* should rescue the senescence phenotype of *Moz*<sup>-/-</sup> MEFs. Indeed, when we cultured *Ink4a-Arf*<sup>-/-</sup>;*Moz*<sup>+/+</sup>, *Ink4a-Arf*<sup>-/-</sup>;*Moz*<sup>+/-</sup> and *Ink4a-Arf*<sup>-/-</sup>;*Moz*<sup>-/-</sup> MEFs, MEFs of all three *Moz* genotypes show similar growth characteristics (Figure 4c,  $p > 0.75$ ,  $n = 5$  independent cultures per genotype), suggesting that MOZ acts through the INK4A-ARF axis to repress cellular senescence.

### ***Cdc6*, *E2f2*, *Ezh2*, *Melk* and *Skp2* are potential targets of MOZ**

We have previously shown that MOZ is a transcriptional activator, and in *Moz*<sup>-/-</sup> embryos, expression of MOZ target genes is reduced by approximately 50%<sup>13, 14</sup>. Therefore, we hypothesized that MOZ regulates the expression of one or more genes encoding upstream repressors of the *Ink4a-Arf* locus rather than repressing the *Ink4a-Arf* locus directly. We examined the expression of known repressors of the *Ink4a-Arf* locus and other senescence mediators identified from the *Moz* microarray (Tables S1-S3).

As expected in *Moz*<sup>-/-</sup> cultures, no *Moz* mRNA was detected (Figure 5a,  $p < 0.001$ ,  $n = 4$  wild type, 4 *Moz*<sup>-/-</sup>). Next, we examined mRNA levels of genes encoding polycomb repressive complex (PRC)1 and PRC2 family members, which are known to directly bind and repress transcription at the *Ink4a-Arf* locus<sup>31-33</sup>. There was no difference in the expression levels of PRC1 genes *Bmi1*, *Mel-18*, *Pcgf2*, *Pcgf3*, *Scmh1* and *Ring1b*

between wild type and *Moz*<sup>-/-</sup> cultures (Figure 5b,  $p > 0.05$ ), while small increases were observed in the levels of *Cbx7*, *Cbx8* and *Ring1a* mRNA ( $p < 0.05$ ). In contrast, the expression of PRC2 member *Ezh2* was reduced by 40% in *Moz*<sup>-/-</sup> cultures (Figure 5c,  $p < 0.001$ ), while *Eed* and *Suz12* were unchanged ( $p > 0.15$ ). Thus, *Ezh2* is the only member of the PRC1 or PRC2 complex that could be responsible for the increase in *Ink4a-Arf* expression levels in the absence of MOZ.

We next analysed three of the eight members of the *E2f* family, *E2f1*, *E2f2* and *E2f3*, which encode proteins essential for the G<sub>1</sub>- to S-phase transition in MEFs<sup>34</sup>. While *E2f1* and *E2f3* mRNA levels were unchanged ( $p > 0.05$ ), a 35% reduction in *E2f2* mRNA in *Moz*<sup>-/-</sup> MEFs was observed (Figure 5d,  $p < 0.001$ ). The cell division cycle associated genes, *Cdca2*<sup>35</sup>, *Cdca8*<sup>36</sup> and *Cdc6*<sup>37, 38</sup>, are all over-expressed in a range of tumour samples, and knockdown of *Cdca2*<sup>35</sup> or *Cdc6*<sup>39</sup> leads to cell cycle arrest. In *Moz*<sup>-/-</sup> MEFs, mRNA levels of *Cdca2*, *Cdca8* and *Cdc6* were all halved compared to wild type (Figure 5e,  $p < 0.001$ ). Lastly, we analysed the expression levels of an array of genes that participate in mediating or maintaining senescence (Figure 5f). Interestingly, mRNA of *Csfl*, which mediates p53-dependent cell cycle arrest<sup>40</sup>, was increased by 45% in *Moz*<sup>-/-</sup> MEFs ( $p = 0.007$ ), while mRNA levels encoding for maternal embryonic leucine-zipper kinase (MELK), which has been shown to mediate the transition of cancer cells from G<sub>1</sub> to S-phase<sup>41</sup>, were halved in *Moz*<sup>-/-</sup> MEFs (Figure 5f,  $p < 0.001$ ). SKP2 mediates cellular senescence by targeting p21<sup>CIP1</sup>, p27<sup>KIP1</sup> and p57<sup>KIP2</sup> for degradation<sup>42-44</sup>. *Skp2* mRNA was reduced by 30% in *Moz*<sup>-/-</sup> MEFs ( $p = 0.001$ ).

Together, our qRT-PCR analysis identified five potential targets that could lead to increased senescence in the absence of MOZ – *Ezh2*, *E2f2*, *Cdc6*, *Melk* and *Skp2*. Expression of these genes was also approximately halved in *Moz*<sup>-/-</sup> MEFs cultured at 3% oxygen, suggesting that these gene expression changes are independent of DNA damage (Figure S6).

### **H3K9 acetylation is reduced in *Moz*<sup>-/-</sup> MEFs at the *Cdc6*, *E2f2*, *Ezh2* and *Melk* loci**

We have previously shown that in the absence of *Moz*, H3K9 acetylation, and not H3K14ac or H4K16ac, is reduced at MOZ target genes *in vivo*<sup>13, 14</sup>. Therefore, we determined whether H3K9ac was reduced at the identified gene loci that are expressed

at low levels in the absence of MOZ and normally repress the *Ink4a-Arf* locus. All ChIP experiments were carried out on subconfluent MEFs one day after passage three.

Compared to wild type, there was a 35% reduction in H3K9ac levels at the transcriptional start site (TSS) of *Cdc6* in *Moz*<sup>-/-</sup> cultures (Figure 6a,  $p < 0.001$ ,  $n = 3$  independent cultures per genotype). Similarly, a 33% reduction in H3K9ac at the TSS of *E2f2* ( $p = 0.003$ ), a 30% reduction at the TSS of *Ezh2* ( $p = 0.023$ ), and a 32% reduction at the TSS of *Melk* ( $p = 0.002$ ) was also observed in *Moz*<sup>-/-</sup> cultures (Figure 6a). In contrast, H3K9ac levels at the TSS of *Skp2* were unchanged ( $p = 0.420$ ). Furthermore, H3K9ac levels at the TSS of our positive control,  $\beta$ -2-microglobulin (*B2m*,  $p = 0.883$ ), and negative control, *Albumin* ( $p = 0.136$ ), were not different between wild type and *Moz*<sup>-/-</sup> samples. Interestingly, the reduction in H3K9ac levels was only evident at the TSS of *Cdc6*, *E2f2*, *Ezh2* and *Melk*, and not 500 bp (three to four nucleosomes) upstream of the TSS (Figure 6b,  $p > 0.05$ ). In contrast to H3K9ac levels, H3K14ac levels were not different between wild type and *Moz*<sup>-/-</sup> samples at the TSS (Figure 6c,  $p > 0.10$ ), or 500 bp upstream of any gene analysed (Figure 6d,  $p > 0.35$ ). These data suggest that in the absence of MOZ, cells are unable to maintain normal levels of H3K9ac levels at the TSS of *Cdc6*, *E2f2*, *Ezh2* and *Melk*, and in turn maintain the required levels of transcription of these genes.

## Discussion

In this study, we have shown that MOZ is an inhibitor, and not a promoter of cellular senescence. Accordingly, *Moz*<sup>-/-</sup> MEFs showed premature senescence due to aberrant and early expression of the *Ink4a-Arf* gene locus. Indeed, on the *Ink4a-Arf*<sup>-/-</sup> background, *Moz*<sup>-/-</sup> MEFs grow as well as wild type MEFs. Through gene expression analysis, we observed that genes normally over-expressed in aggressive and highly proliferative cancers were expressed at low levels in *Moz*-deficient MEFs. In addition, we show that known inhibitors of *Ink4a-Arf* expression, namely *Cdc6*, *Ezh2* and *E2f2*, were expressed at low levels in *Moz*-deficient MEFs. Our data strongly suggest that MOZ is an upstream inhibitor of the INK4A-ARF pathway.

Senescence is important for inhibiting the over-proliferation of cells and plays a pivotal role in preventing and restraining tumour growth<sup>45-47</sup>. Products of the *Ink4a-Arf* locus, p16<sup>INK4A</sup> and p19<sup>ARF</sup> are potent inhibitors of senescence<sup>30</sup>, and are commonly mutated and inactivated in human cancers<sup>48</sup>. The *Ink4a-Arf* locus is alternatively spliced to produce two protein products in mice, p16<sup>INK4A</sup> and p19<sup>ARF(49)</sup>. P16<sup>INK4A</sup> retards the cycling of cells by directly binding and inhibiting cyclin dependent kinase 4 (CDK4) and cyclin D<sup>50</sup>, thereby retaining cells in G<sub>1</sub>-phase of the cell cycle<sup>51</sup>. P19<sup>ARF</sup> sequesters MDM2, an inhibitor of p53, and promotes senescence by releasing p53<sup>52</sup>. Genes under-expressed in the absence of MOZ are strongly expressed in cancer. Indeed, CDC6 was found to be strongly expressed in 50% of brain tumours<sup>37</sup> and in 50% of non-small-cell lung carcinomas<sup>38</sup>, while knockdown of *CDC6* in HeLa cells lead to cell cycle arrest<sup>39</sup>. Similarly, high levels of EZH2 protein in human melanoma, prostate, uterine and breast cancers correlate with an aggressive tumour phenotype and poor prognosis<sup>53-55</sup>. In contrast, knockdown of *EZH2* in the PC3 prostate cancer line was able to markedly reduce proliferation<sup>55</sup>. The role of E2F2 in cancer is much more complex, as E2F2 can act as both an oncogene or tumour suppressor depending on the cancer model and the context in which it is tested<sup>56</sup>. Nevertheless, in MEFs, knockout models of *E2f1* to 3 show a reduction in proliferation in a functionally redundant manner<sup>34</sup>, suggesting a role for E2Fs in the G<sub>1</sub> to S-phase transition. Importantly, CDC6<sup>57</sup> and EZH2<sup>31</sup> have been shown to directly stall senescence by repressing the *Ink4a-Arf* locus, while E2F2 is likely to indirectly repress *Ink4a-Arf* through its ability to activate *Cdc6*<sup>58</sup> and *Ezh2*<sup>59</sup> expression. The role of MELK is less well established. However, MELK has been shown to regulate the self-renewal of neural progenitors<sup>60</sup>, is highly expressed in brain tumours, and high MELK expression correlates with a poor prognosis<sup>61</sup>. Indeed, knockdown of *MELK* in cancer cell lines leads to a decrease in proliferation<sup>41, 61</sup> and cell cycle arrest in G<sub>1</sub>-phase<sup>41</sup>. These observations are consistent with our data indicating that genes normally overexpressed in cancers were expressed at low levels in *Moz*<sup>-/-</sup> MEFs (Figure 3).

The premature senescence identified in *Moz*-knockout cells in this study is more severe than cells that only lack the catalytic activity of MOZ<sup>16</sup>. Nevertheless, our data are largely in agreement with the Perez-Campo study showing that MOZ is required to suppress senescence<sup>16</sup>, although we favour a model in which MOZ acts as an activator

of gene expression, specifically of genes coding for inhibitors of senescence. However, it has also been shown that in response to DNA damage, *Moz*<sup>-/-</sup> MEFs are unable to induce *p21* expression to the same levels as wild type controls and are unable to senesce<sup>15</sup>. While this is difficult to reconcile with our results, one possibility is that in the abovementioned study<sup>15</sup>, *Moz*<sup>-/-</sup> MEFs may have been in an advanced state of cellular senescence due to de-repression of the *Ink4a-Arf* locus described here. If this were the case, normal levels of p21<sup>CIP1</sup> would not be expected upon UV-irradiation, as a smaller number of *Moz*<sup>-/-</sup> MEFs would be cycling and most would already be arrested. Rokudai and co-workers have also shown that over-expressed MOZ binds to p53, acetylates p53 at K120 and K382 in cell free assays and together with p53, activates the expression of *p21* in response to DNA damage<sup>15, 62</sup>. These studies suggest that in response to DNA damage, MOZ acts as an activator and not a repressor of senescence. While we can not rule out that MOZ, like other chromatin modifying complexes, may act via different mechanisms depending on the cellular context (i.e. induced DNA damage versus untreated MEFs), conclusions based on overexpression experiments and cell-free assays must be carefully considered. For instance, in cell-free assays, MOZ is able to acetylate histone H3, H4 and H2A<sup>12, 63</sup>. In contrast, when the complete MOZ/MORF-ING5 complex is incubated with oligonucleosomes, MOZ specifically acetylates H3K14<sup>64</sup>, while in *Moz*<sup>-/-</sup> embryos, a specific reduction in H3K9ac and not H3K14ac at MOZ target genes is observed<sup>13, 14</sup>.

In conclusion, we have established that MOZ represses cellular senescence in MEFs while not affecting apoptosis or DNA damage. Through gene expression analysis, we have shown that in the absence of MOZ, there is a reduction in the mRNA levels of genes that inhibit senescence including *Cdc6*, *E2f2*, *Ezh2* and *Melk*, and that H3K9ac levels are reduced at the TSS of these genes. Altogether, this work establishes MOZ as a key inhibitor of senescence at the level of chromatin regulation and gene transcription.

## Materials and Methods

### Animals

All mice were maintained on a C57BL/6 background. The *Moz*<sup>-</sup> allele<sup>13</sup> and the *Ink4a-Arf* mutant mice<sup>30</sup> have been previously described. All experiments were performed under approval from the Walter and Eliza Hall Institute's Animal Ethics Committee.

### Cell culture proliferation, cell death, and senescence assays

MEFs were isolated and cultured from E12.5 embryos of *Moz*<sup>+/-</sup> intercrosses. MEFs were plated at a density of 12,500 cells/cm<sup>2</sup>. Subconfluent MEFs were treated with BrdU (Sigma, B5002) and stained with anti-BrdU antibody (1:10, Clone Bu20a, Dako M0744), followed by detection with a fluorescent secondary antibody as described previously<sup>14</sup>. MEFs were counterstained with Hoechst 33258 and counted. DAPI/Ki67 staining was carried out using one million subconfluent MEFs using the BD Cytofix/Cytoperm kit (BD Biosciences, 554714), and the Ki67-FITC antibody (BD Bioscience, 556026) as per manufacturer's instructions. For viability assays, cells were analysed by flow cytometry by staining with propidium iodide and FITC-conjugated annexin V (Life Technologies A13199, 1:200).  $\beta$ -galactosidase staining and analysis were carried out on subconfluent MEFs as described<sup>65</sup>.  $\gamma$ H2A.X staining was performed using the BD Cytofix/Cytoperm kit (BD Biosciences, 554714), and a  $\gamma$ H2A.X-biotin conjugated antibody (1:400, Millipore 16-193) and was detected using APC-streptavidin and flow cytometry essentially as described by<sup>21</sup>. O<sub>2</sub>•<sup>-</sup> production was measured by staining with 10  $\mu$ g/ml dihydroethidium and 2  $\mu$ g/ml Hoechst-33258 at 37°C for 30 min. The ratio of DHE to Hoechst used to determine O<sub>2</sub>•<sup>-</sup> production.

### Gene expression analysis

RNA was isolated from wild type, *Moz*<sup>+/-</sup> and *Moz*<sup>-/-</sup> MEFs one day after passage 3 and hybridized to Illumina MouseWG-6 v2.0 BeadChips at the Australian Genome Research Facility. Intensity values were *neqc* normalised<sup>66</sup>. Probes were filtered if they failed to be detected (P<0.01) on any array. First, the *Moz*<sup>+/-</sup> and *Moz*<sup>-/-</sup> cultures were each compared to wild type. Second, the expression of each gene was regressed on a covariate representing the degree of *Moz*-deficiency (wild type = 0, *Moz*<sup>+/-</sup> = 0.2, *Moz*<sup>-/-</sup> = 1). Differential expression was assessed using empirical Bayes moderated t-statistics<sup>67</sup>.

The CAMERA procedure<sup>68</sup> was used to test whether signatures in the C2 collection of the Molecular Signatures Database<sup>69</sup> were correlated with *Moz*-deficiency. Proliferation, apoptosis and senescence gene sets were further tested using ROAST gene set tests<sup>70</sup>.

Genes differentially expressed in *Zmpste24*<sup>-/-</sup> MEFs were determined from a previously published study<sup>22</sup>. Probe-sets showing 2-fold change or more after gcRMA normalization<sup>71</sup> were considered to be differentially expressed.

Quantitative RT-PCR was carried out using the LightCycler 480 (Roche) and SYBR green chemistry (Table S5). Western blot analyses were performed using antibodies raised against p21<sup>CIP1</sup> (Santa Cruz c-19, sc-397), p19<sup>ARF</sup> (Abcam, ab80), p16<sup>INK4A</sup> (Santa Cruz M156, sc-1207) and detected using an anti-rabbit IgG-HRP conjugated antibody (GE Healthcare NA934v). Actin loading control was detected using an Actin-HRP conjugated antibody (Santa Cruz, sc-1616)

### **Chromatin Immunoprecipitation (ChIP)**

ChIP was carried out as previously described<sup>72</sup> with two million subconfluent MEFs per sample. Immunoprecipitation was carried out using 5 µg of H3K9ac (Cell signaling, #9649S) and H3K14ac (Cell signaling, #7627) antibodies. Primer sequences are provided in Table S6.

### **Statistical Analysis**

Statistical analyses were carried out using the Stata v12 software (Stata Corporation, USA). Data were analysed using ANOVA followed by Bonferroni's post-hoc test. Data are presented as mean ± s.e.m.

### **Acknowledgements**

We thank Rose Cobb, Carmen Gatt and Faye Dabrowski for technical support. We thank Andreas Strasser for helpful discussions and Liz Valente for the provision of the anti-p21<sup>CIP1</sup> antibody. This work was supported by the Australian National Health and Medical Research Council (senior research fellowships to A.K.V. and T.T.; scholarship to B.N.S.), the Australian Mitochondrial Disease Foundation (M.J.B.), Australian Postgraduate Awards (to M.J.B., F.E., H.K.V.), and operational infrastructure grants

from the Australian Federal Government (IRISS) and the Victorian State Government (OIS).

## References

1. Borrow J, Stanton VP, Jr., Andresen JM, Becher R, Behm FG, Chaganti RS *et al.* The translocation t(8;16)(p11;p13) of acute myeloid leukaemia fuses a putative acetyltransferase to the CREB-binding protein. *Nat Genet* 1996; 14: 33-41.
2. Sun T, Wu E. Acute monoblastic leukemia with t(8;16): a distinct clinicopathologic entity; report of a case and review of the literature. *Am J Hematol* 2001; 66: 207-212.
3. Stark B, Resnitzky P, Jeison M, Luria D, Blau O, Avigad S *et al.* A distinct subtype of M4/M5 acute myeloblastic leukemia (AML) associated with t(8;16)(p11:p13), in a patient with the variant t(8;19)(p11;q13)--case report and review of the literature. *Leuk Res* 1995; 19: 367-379.
4. Haferlach T, Kohlmann A, Klein HU, Ruckert C, Dugas M, Williams PM *et al.* AML with translocation t(8;16)(p11;p13) demonstrates unique cytomorphological, cytogenetic, molecular and prognostic features. *Leukemia* 2009; 23: 934-943.
5. Camos M, Esteve J, Jares P, Colomer D, Rozman M, Villamor N *et al.* Gene expression profiling of acute myeloid leukemia with translocation t(8;16)(p11;p13) and MYST3-CREBBP rearrangement reveals a distinctive signature with a specific pattern of HOX gene expression. *Cancer Res* 2006; 66: 6947-6954.
6. Carapeti M, Aguiar RC, Goldman JM, Cross NC. A novel fusion between MOZ and the nuclear receptor coactivator TIF2 in acute myeloid leukemia. *Blood* 1998; 91: 3127-3133.
7. Chaffanet M, Gressin L, Preudhomme C, Soenen-Cornu V, Birnbaum D, Pebusque MJ. MOZ is fused to p300 in an acute monocytic leukemia with t(8;22). *Genes Chromosomes Cancer* 2000; 28: 138-144.
8. Esteyries S, Perot C, Adelaide J, Imbert M, Lagarde A, Pautas C *et al.* NCOA3, a new fusion partner for MOZ/MYST3 in M5 acute myeloid leukemia. *Leukemia* 2008; 22: 663-665.
9. Huntly BJ, Shigematsu H, Deguchi K, Lee BH, Mizuno S, Duclos N *et al.* MOZ-TIF2, but not BCR-ABL, confers properties of leukemic stem cells to committed murine hematopoietic progenitors. *Cancer Cell* 2004; 6: 587-596.

10. Thomas T, Corcoran LM, Gugasyan R, Dixon MP, Brodnicki T, Nutt SL *et al.* Monocytic leukemia zinc finger protein is essential for the development of long-term reconstituting hematopoietic stem cells. *Genes Dev* 2006; 20: 1175-1186.
11. Katsumoto T, Aikawa Y, Iwama A, Ueda S, Ichikawa H, Ochiya T *et al.* MOZ is essential for maintenance of hematopoietic stem cells. *Genes Dev* 2006; 20: 1321-1330.
12. Perez-Campo FM, Borrow J, Kouskoff V, Lacaud G. The histone acetyl transferase activity of monocytic leukemia zinc finger is critical for the proliferation of hematopoietic precursors. *Blood* 2009; 113: 4866-4874.
13. Voss AK, Collin C, Dixon MP, Thomas T. Moz and retinoic acid coordinately regulate H3K9 acetylation, Hox gene expression, and segment identity. *Dev Cell* 2009; 17: 674-686.
14. Voss AK, Vanyai HK, Collin C, Dixon MP, McLennan TS, Sheikh BN *et al.* MOZ regulates the Tbx1 locus, and Moz mutation partially phenocopies DiGeorge syndrome. *Dev Cell* 2012; 23: 652-663.
15. Rokudai S, Aikawa Y, Tagata Y, Tsuchida N, Taya Y, Kitabayashi I. Monocytic leukemia zinc finger (MOZ) interacts with p53 to induce p21 expression and cell-cycle arrest. *J Biol Chem* 2009; 284: 237-244.
16. Perez-Campo FM, Costa G, Lie ALM, Stifani S, Kouskoff V, Lacaud G. MOZ-mediated repression of p16 is critical for the self-renewal of neural and hematopoietic stem cells. *Stem Cells* 2013.
17. Dimri GP, Lee X, Basile G, Acosta M, Scott G, Roskelley C *et al.* A biomarker that identifies senescent human cells in culture and in aging skin in vivo. *Proc Natl Acad Sci U S A* 1995; 92: 9363-9367.
18. Lu T, Finkel T. Free radicals and senescence. *Exp Cell Res* 2008; 314: 1918-1922.
19. Parrinello S, Samper E, Krtolica A, Goldstein J, Melov S, Campisi J. Oxygen sensitivity severely limits the replicative lifespan of murine fibroblasts. *Nat Cell Biol* 2003; 5: 741-747.
20. Rogakou EP, Pilch DR, Orr AH, Ivanova VS, Bonner WM. DNA double-stranded breaks induce histone H2AX phosphorylation on serine 139. *J Biol Chem* 1998; 273: 5858-5868.
21. Muslimovic A, Ismail IH, Gao Y, Hammarsten O. An optimized method for measurement of gamma-H2AX in blood mononuclear and cultured cells. *Nat Protoc* 2008; 3: 1187-1193.

22. Liu B, Wang J, Chan KM, Tjia WM, Deng W, Guan X *et al.* Genomic instability in laminopathy-based premature aging. *Nat Med* 2005; 11: 780-785.
23. Tang X, Milyavsky M, Goldfinger N, Rotter V. Amyloid-beta precursor-like protein APLP1 is a novel p53 transcriptional target gene that augments neuroblastoma cell death upon genotoxic stress. *Oncogene* 2007; 26: 7302-7312.
24. Vasseur S, Malicet C, Calvo EL, Labrie C, Berthezene P, Dagorn JC *et al.* Gene expression profiling by DNA microarray analysis in mouse embryonic fibroblasts transformed by rasV12 mutated protein and the E1A oncogene. *Mol Cancer* 2003; 2: 19.
25. Ben-Porath I, Thomson MW, Carey VJ, Ge R, Bell GW, Regev A *et al.* An embryonic stem cell-like gene expression signature in poorly differentiated aggressive human tumors. *Nat Genet* 2008; 40: 499-507.
26. Chiang DY, Villanueva A, Hoshida Y, Peix J, Newell P, Minguez B *et al.* Focal gains of VEGFA and molecular classification of hepatocellular carcinoma. *Cancer Res* 2008; 68: 6779-6788.
27. Sherr CJ. The INK4a/ARF network in tumour suppression. *Nat Rev Mol Cell Biol* 2001; 2: 731-737.
28. Besson A, Dowdy SF, Roberts JM. CDK inhibitors: cell cycle regulators and beyond. *Dev Cell* 2008; 14: 159-169.
29. Maddika S, Ande SR, Panigrahi S, Paranjothy T, Weglarczyk K, Zuse A *et al.* Cell survival, cell death and cell cycle pathways are interconnected: implications for cancer therapy. *Drug Resist Updat* 2007; 10: 13-29.
30. Serrano M, Lee H, Chin L, Cordon-Cardo C, Beach D, DePinho RA. Role of the INK4a locus in tumor suppression and cell mortality. *Cell* 1996; 85: 27-37.
31. Agherbi H, Gaussmann-Wenger A, Verthuy C, Chasson L, Serrano M, Djabali M. Polycomb mediated epigenetic silencing and replication timing at the INK4a/ARF locus during senescence. *PLoS One* 2009; 4: e5622.
32. Maertens GN, El Messaoudi-Aubert S, Racek T, Stock JK, Nicholls J, Rodriguez-Niedenfuhr M *et al.* Several distinct polycomb complexes regulate and co-localize on the INK4a tumor suppressor locus. *PLoS One* 2009; 4: e6380.
33. Dietrich N, Bracken AP, Trinh E, Schjerling CK, Koseki H, Rappsilber J *et al.* Bypass of senescence by the polycomb group protein CBX8 through direct binding to the INK4A-ARF locus. *EMBO J* 2007; 26: 1637-1648.

34. Wu L, Timmers C, Maiti B, Saavedra HI, Sang L, Chong GT *et al.* The E2F1-3 transcription factors are essential for cellular proliferation. *Nature* 2001; 414: 457-462.
35. Uchida F, Uzawa K, Kasamatsu A, Takatori H, Sakamoto Y, Ogawara K *et al.* Overexpression of CDCA2 in human squamous cell carcinoma: correlation with prevention of G1 phase arrest and apoptosis. *PLoS One* 2013; 8: e56381.
36. Hayama S, Daigo Y, Yamabuki T, Hirata D, Kato T, Miyamoto M *et al.* Phosphorylation and activation of cell division cycle associated 8 by aurora kinase B plays a significant role in human lung carcinogenesis. *Cancer Res* 2007; 67: 4113-4122.
37. Ohta S, Koide M, Tokuyama T, Yokota N, Nishizawa S, Namba H. Cdc6 expression as a marker of proliferative activity in brain tumors. *Oncol Rep* 2001; 8: 1063-1066.
38. Karakaidos P, Taraviras S, Vassiliou LV, Zacharatos P, Kastrinakis NG, Kougiou D *et al.* Overexpression of the replication licensing regulators hCdt1 and hCdc6 characterizes a subset of non-small-cell lung carcinomas: synergistic effect with mutant p53 on tumor growth and chromosomal instability--evidence of E2F-1 transcriptional control over hCdt1. *Am J Pathol* 2004; 165: 1351-1365.
39. Lau E, Zhu C, Abraham RT, Jiang W. The functional role of Cdc6 in S-G2/M in mammalian cells. *EMBO Rep* 2006; 7: 425-430.
40. Azzam G, Wang X, Bell D, Murphy ME. CSF1 Is a Novel p53 Target Gene Whose Protein Product Functions in a Feed-Forward Manner to Suppress Apoptosis and Enhance p53-Mediated Growth Arrest. *PLoS One* 2013; 8: e74297.
41. Kig C, Beullens M, Beke L, Van Eynde A, Linders JT, Brehmer D *et al.* Maternal Embryonic Leucine Zipper Kinase (MELK) Reduces Replication Stress in Glioblastoma Cells. *J Biol Chem* 2013; 288: 24200-24212.
42. Bornstein G, Bloom J, Sitry-Shevah D, Nakayama K, Pagano M, Hershko A. Role of the SCFSkp2 ubiquitin ligase in the degradation of p21Cip1 in S phase. *J Biol Chem* 2003; 278: 25752-25757.
43. Carrano AC, Eytan E, Hershko A, Pagano M. SKP2 is required for ubiquitin-mediated degradation of the CDK inhibitor p27. *Nat Cell Biol* 1999; 1: 193-199.
44. Kamura T, Hara T, Kotoshiba S, Yada M, Ishida N, Imaki H *et al.* Degradation of p57Kip2 mediated by SCFSkp2-dependent ubiquitylation. *Proc Natl Acad Sci U S A* 2003; 100: 10231-10236.

45. Reimann M, Lee S, Loddenkemper C, Dorr JR, Tabor V, Aichele P *et al.* Tumor stroma-derived TGF-beta limits myc-driven lymphomagenesis via Suv39h1-dependent senescence. *Cancer Cell* 2010; 17: 262-272.
46. Chen Z, Trotman LC, Shaffer D, Lin HK, Dotan ZA, Niki M *et al.* Crucial role of p53-dependent cellular senescence in suppression of Pten-deficient tumorigenesis. *Nature* 2005; 436: 725-730.
47. Braig M, Lee S, Loddenkemper C, Rudolph C, Peters AH, Schlegelberger B *et al.* Oncogene-induced senescence as an initial barrier in lymphoma development. *Nature* 2005; 436: 660-665.
48. Kamb A, Gruis NA, Weaver-Feldhaus J, Liu Q, Harshman K, Tavtigian SV *et al.* A cell cycle regulator potentially involved in genesis of many tumor types. *Science* 1994; 264: 436-440.
49. Quelle DE, Zindy F, Ashmun RA, Sherr CJ. Alternative reading frames of the INK4a tumor suppressor gene encode two unrelated proteins capable of inducing cell cycle arrest. *Cell* 1995; 83: 993-1000.
50. Serrano M, Hannon GJ, Beach D. A new regulatory motif in cell-cycle control causing specific inhibition of cyclin D/CDK4. *Nature* 1993; 366: 704-707.
51. Koh J, Enders GH, Dynlacht BD, Harlow E. Tumour-derived p16 alleles encoding proteins defective in cell-cycle inhibition. *Nature* 1995; 375: 506-510.
52. Weber JD, Taylor LJ, Roussel MF, Sherr CJ, Bar-Sagi D. Nucleolar Arf sequesters Mdm2 and activates p53. *Nat Cell Biol* 1999; 1: 20-26.
53. Bachmann IM, Halvorsen OJ, Collett K, Stefansson IM, Straume O, Haukaas SA *et al.* EZH2 expression is associated with high proliferation rate and aggressive tumor subgroups in cutaneous melanoma and cancers of the endometrium, prostate, and breast. *J Clin Oncol* 2006; 24: 268-273.
54. Klee CG, Cao Q, Varambally S, Shen R, Ota I, Tomlins SA *et al.* EZH2 is a marker of aggressive breast cancer and promotes neoplastic transformation of breast epithelial cells. *Proc Natl Acad Sci U S A* 2003; 100: 11606-11611.
55. Varambally S, Dhanasekaran SM, Zhou M, Barrette TR, Kumar-Sinha C, Sanda MG *et al.* The polycomb group protein EZH2 is involved in progression of prostate cancer. *Nature* 2002; 419: 624-629.
56. Chen HZ, Tsai SY, Leone G. Emerging roles of E2Fs in cancer: an exit from cell cycle control. *Nat Rev Cancer* 2009; 9: 785-797.

57. Gonzalez S, Klatt P, Delgado S, Conde E, Lopez-Rios F, Sanchez-Cespedes M *et al.* Oncogenic activity of Cdc6 through repression of the INK4/ARF locus. *Nature* 2006; 440: 702-706.
58. Yan Z, DeGregori J, Shohet R, Leone G, Stillman B, Nevins JR *et al.* Cdc6 is regulated by E2F and is essential for DNA replication in mammalian cells. *Proc Natl Acad Sci U S A* 1998; 95: 3603-3608.
59. Bracken AP, Pasini D, Capra M, Prosperini E, Colli E, Helin K. EZH2 is downstream of the pRB-E2F pathway, essential for proliferation and amplified in cancer. *EMBO J* 2003; 22: 5323-5335.
60. Nakano I, Paucar AA, Bajpai R, Dougherty JD, Zewail A, Kelly TK *et al.* Maternal embryonic leucine zipper kinase (MELK) regulates multipotent neural progenitor proliferation. *J Cell Biol* 2005; 170: 413-427.
61. Nakano I, Masterman-Smith M, Saigusa K, Paucar AA, Horvath S, Shoemaker L *et al.* Maternal embryonic leucine zipper kinase is a key regulator of the proliferation of malignant brain tumors, including brain tumor stem cells. *J Neurosci Res* 2008; 86: 48-60.
62. Rokudai S, Laptenko O, Arnal SM, Taya Y, Kitabayashi I, Prives C. MOZ increases p53 acetylation and premature senescence through its complex formation with PML. *Proc Natl Acad Sci U S A* 2013; 110: 3895-3900.
63. Champagne N, Pelletier N, Yang XJ. The monocytic leukemia zinc finger protein MOZ is a histone acetyltransferase. *Oncogene* 2001; 20: 404-409.
64. Doyon Y, Cayrou C, Ullah M, Landry AJ, Cote V, Selleck W *et al.* ING tumor suppressor proteins are critical regulators of chromatin acetylation required for genome expression and perpetuation. *Mol Cell* 2006; 21: 51-64.
65. Debacq-Chainiaux F, Erusalimsky JD, Campisi J, Toussaint O. Protocols to detect senescence-associated beta-galactosidase (SA-beta-gal) activity, a biomarker of senescent cells in culture and in vivo. *Nat Protoc* 2009; 4: 1798-1806.
66. Shi W, Oshlack A, Smyth GK. Optimizing the noise versus bias trade-off for Illumina whole genome expression BeadChips. *Nucleic Acids Res* 2010; 38: e204.
67. Smyth GK. Linear models and empirical bayes methods for assessing differential expression in microarray experiments. *Stat Appl Genet Mol Biol* 2004; 3: Article3.
68. Wu D, Smyth GK. Camera: a competitive gene set test accounting for inter-gene correlation. *Nucleic Acids Res* 2012; 40: e133.

69. Liberzon A, Subramanian A, Pinchback R, Thorvaldsdottir H, Tamayo P, Mesirov JP. Molecular signatures database (MSigDB) 3.0. *Bioinformatics* 2011; 27: 1739-1740.
70. Wu D, Lim E, Vaillant F, Asselin-Labat ML, Visvader JE, Smyth GK. ROAST: rotation gene set tests for complex microarray experiments. *Bioinformatics* 2010; 26: 2176-2182.
71. Wu Z, Irizarry R, Gentleman R, Martinez-Murillo F, Spencer F. A Model-Based Background Adjustment for Oligonucleotide Expression Arrays. *Journal of the American Statistical Association* 2004; 99: 909.
72. Voss AK, Dixon MP, McLennan T, Kueh AJ, Thomas T. Chromatin immunoprecipitation of mouse embryos. *Methods Mol Biol* 2012; 809: 335-352.

## Figure Legends

**Figure 1** – *Moz* mutant MEFs display premature senescence.

(a) Cell numbers in cultures of primary wild type (n = 4), *Moz*<sup>+/-</sup> (n = 3), and *Moz*<sup>-/-</sup> (n = 5) MEFs. Cell numbers in *Moz*<sup>-/-</sup> cultures were reduced from passage 3. (b) Detection of senescence associated  $\beta$ -galactosidase activity in passage 3 MEFs. Note the strong staining in *Moz*<sup>-/-</sup> (n = 3) and not wild type (n = 5) MEFs. (c) Quantification of  $\beta$ -galactosidase activity by flow cytometry between passages 2 and 5. Compared to wild type (n = 5), there was a significant increase in senescence associated  $\beta$ -galactosidase activity in *Moz*<sup>-/-</sup> cultures (n = 3) from passage 2, and in *Moz*<sup>+/-</sup> cultures (n = 4) from passage 4 (FACS plots in Figure S1). (d) ROS ( $O_2^{\bullet-}$ ) production in passage 3 fibroblasts. ROS levels were higher *Moz*<sup>-/-</sup> (n = 11) versus wild type (n = 6) cultures. Data are a combination of 3 independent experiments. (e) mRNA expression of senescence marker genes *Ink4a*, *Arf* and *Ink4b*, which were all significantly increased in passage 5 *Moz*<sup>-/-</sup> cultures (n = 3) compared to wild type (n = 2). (f) BrdU incorporation at passages 2 and 4 to quantify cells undergoing DNA synthesis, showing a decrease in BrdU incorporation at passage 4 in *Moz*<sup>-/-</sup> cultures. n = 4 wild type and 5 *Moz*<sup>-/-</sup> cultures. (g) Quantification of apoptotic cell death over 3 days after passages 2, 4 and 6 by annexin V and flow cytometry. Cell death was similar in wild type and *Moz*<sup>-/-</sup> cultures. n = 5 wild type, 4 *Moz*<sup>+/-</sup> and 3 *Moz*<sup>-/-</sup> cultures at each time point.

Asterisks indicate a statistically significant difference between the marked genotype and wild type at \**p* < 0.05, \*\**p* < 0.01, and \*\*\**p* < 0.001. Scale bars in (B) equal 200  $\mu$ m.

**Figure 2** – Premature senescence in *Moz*<sup>-/-</sup> MEFs is independent of DNA damage.

(a) Immunofluorescence detection of  $\gamma$ H2A.X (red) marking double stranded DNA breaks in the nucleus (blue, Hoechst 33258). (b) Quantification of double stranded DNA breaks at passages 1, 3 and 5 by  $\gamma$ H2A.X staining in MEFs cultured at 20% O<sub>2</sub>. Analyses were carried out by flow cytometry. MEFs were separated based on DNA content to ensure an accurate analysis (FACS plots in Figure S3). n = 5 wild type, 4 *Moz*<sup>+/-</sup> and 3 *Moz*<sup>-/-</sup> cultures at each passage. (c) Proliferation curves of primary MEFs cultured at physiological (3%) oxygen. There were fewer MEFs in *Moz*<sup>-/-</sup> cultures from passage 6, and fewer MEFs in *Moz*<sup>+/-</sup> cultures from passage 8. (d) qRT-PCR analysis of MEFs grown at 3% O<sub>2</sub> at passage 5 showing an increase in senescence markers *Ink4a*, *Arf* and *Ink4b*. n = 4 wild type and 4 *Moz*<sup>-/-</sup> cultures. (e) Analysis of BrdU incorporation at passages 2 and 5 in primary MEFs grown at 3% O<sub>2</sub>. There was a reduction in BrdU incorporation in *Moz*<sup>-/-</sup> cultures (n = 5) compared to wild type cultures (n = 4), showing a decrease in cells undergoing DNA synthesis. (f) Quantification of apoptotic cell death over 3 days after passages 2, 5 and 7 by annexin V staining and flow cytometry. n = 4 wild type, 3 *Moz*<sup>+/-</sup> and 5 *Moz*<sup>-/-</sup> cultures at each time point.

Asterisks indicate a statistically significant difference between the marked genotype and wild type at \**p* < 0.05, \*\**p* < 0.01, and \*\*\**p* < 0.001.

**Figure 3** – Expression profiling of *Moz* mutant MEFs.

(a) Experimental design used to interrogate mRNA expression levels in passage 3 wild type and *Moz* mutant MEFs. (b) Venn diagram showing the number of significantly up-regulated and down-regulated genes in *Moz*<sup>-/-</sup> and *Moz*<sup>+/-</sup> cultures compared to wild type. A false discovery rate cut-off of 10% was used. The full gene lists for these comparisons can be found in Tables S1 and S2. *Moz*<sup>+/-</sup> cultures were more similar to wild type at passage 3 compared to *Moz*<sup>-/-</sup> cultures. Analysis of genes showing an intermediate phenotype in *Moz*<sup>+/-</sup> cultures compared to wild type and *Moz*<sup>-/-</sup> can be found in Table S3. This gene list was used for subsequent gene-set analysis. (c,d,e) Gene-set analysis comparing the *Moz* dataset to published microarray studies analysing senescence (c), proliferation (d) and apoptosis (e). Consistent with the phenotype of *Moz* mutant MEFs, genes up-regulated during p53-mediated senescence and in the premature aging model of *Zmpste24*<sup>-/-</sup> MEFs were expressed at high levels in *Moz*<sup>-/-</sup>

MEFs. In contrast, genes down-regulated during senescence were enriched in *Moz* wild type MEFs. The *Moz* dataset did not show any correlation with oncogene (RASV12) induced senescence or apoptosis. Genes up-regulated in proliferating cells were enriched in *Moz* wild type, and not *Moz*-mutant MEFs. **(f)** Gene-set analysis comparing the *Moz* dataset to datasets available through the Broad Institute. The 30 gene-sets showing the strongest correlation to the *Moz* dataset are provided here. A full list can be found in Table S4. n = 2 independent cultures of each genotype. *p*-values as indicated in Figure.

**Figure 4** – Analysis of senescence mediators in *Moz*<sup>-/-</sup> MEFs in 20% oxygen.

**(a)** mRNA expression levels of the *Ink4* family genes encoding regulators of proliferation and senescence, showing a significant increase in expression from the *Ink4a-Arf-Ink4b* locus. n = 4 wild type and 4 *Moz*<sup>-/-</sup> cultures. **(b)** mRNA levels of genes encoding the CIP-KIP family of cell cycle regulators. n = 4 wild type and 4 *Moz*<sup>-/-</sup> cultures. **(c)** Proliferation curves of wild type, *Moz*<sup>+/-</sup> and *Moz*<sup>-/-</sup> MEFs on an *Ink4a-Arf* null background. There were no differences in the number of MEFs across the three genotypes at all passages. n = 5 cultures of each genotype.

All MEFs were grown at atmospheric (20%) O<sub>2</sub>. qRT-PCR analyses were carried out on subconfluent MEFs 24 hours after passage 3. Asterisks indicate a statistically significant difference between the marked genotype and wild type at \**p* < 0.05, \*\**p* < 0.01, and \*\*\**p* < 0.001.

**Figure 5** – Analysis of regulators of senescence and cell proliferation in *Moz*-deficient MEFs.

**(a)** *Moz* mRNA was not detected in *Moz*<sup>-/-</sup> MEFs. **(b)** mRNA expression analysis of the polycomb repressive complex 1 (PRC1) genes. No decrease in the mRNA levels of any PRC1 genes was found in *Moz*<sup>-/-</sup> MEFs. An increase in *Cbx7*, *Cbx8* and *Ring1a* was observed. **(c)** Expression levels of PRC2 member genes. *Ezh2* mRNA levels were approximately halved in *Moz*<sup>-/-</sup> MEFs. **(d)** mRNA levels of *Myc* and its downstream target genes *E2f1*, *E2f2* and *E2f3*, the protein products of which regulate cell cycle progression. *E2f2* mRNA was significantly reduced. **(e)** Analysis of cell division cycle (*Cdc*) genes that were significantly reduced in the *Moz*<sup>-/-</sup> MEF microarray. CDC proteins regulate the progression of the cell cycle, while CDC6 also directly represses the *Ink4a-Arf* locus. Expression levels of *Cdca2*, *Cdca8*, and *Cdc6* were halved in *Moz*<sup>-/-</sup>

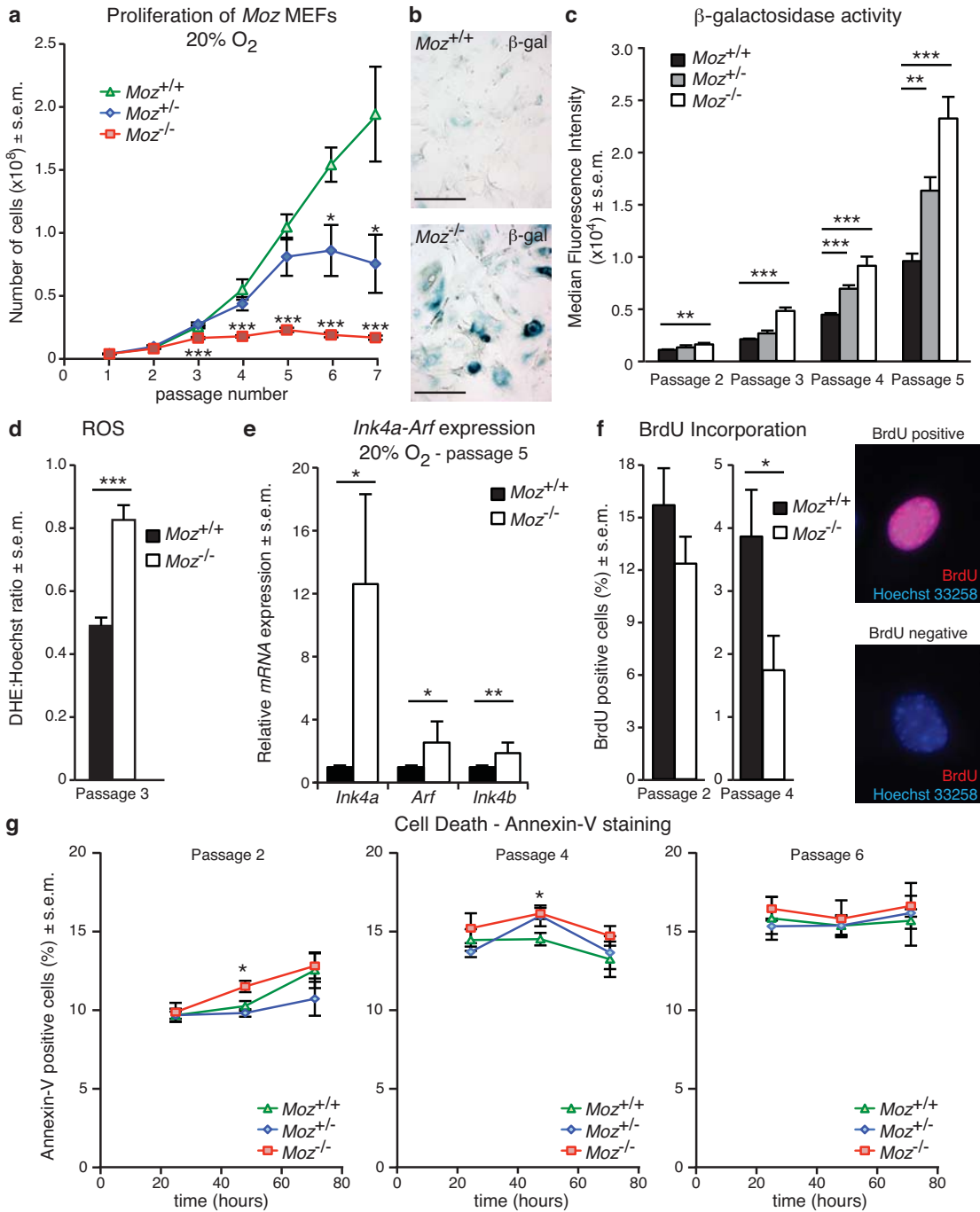
MEFs. (f) mRNA analysis of senescence mediators. Only *Melk* and *Skp2* mRNA were significantly reduced in *Moz*<sup>-/-</sup> MEFs.

All MEFs used for qRT-PCR analysis were grown at atmospheric (20%) O<sub>2</sub> (Corresponding data for cultures in 3% O<sub>2</sub> in Figure S6). Analyses were carried out on subconfluent MEFs 24 hours after passage 3. Asterisks indicate a statistically significant difference between the marked genotype and wild type at \**p* < 0.05, \*\**p* < 0.01, and \*\*\**p* < 0.001. n = 4 wild type and 4 *Moz*<sup>-/-</sup> cultures.

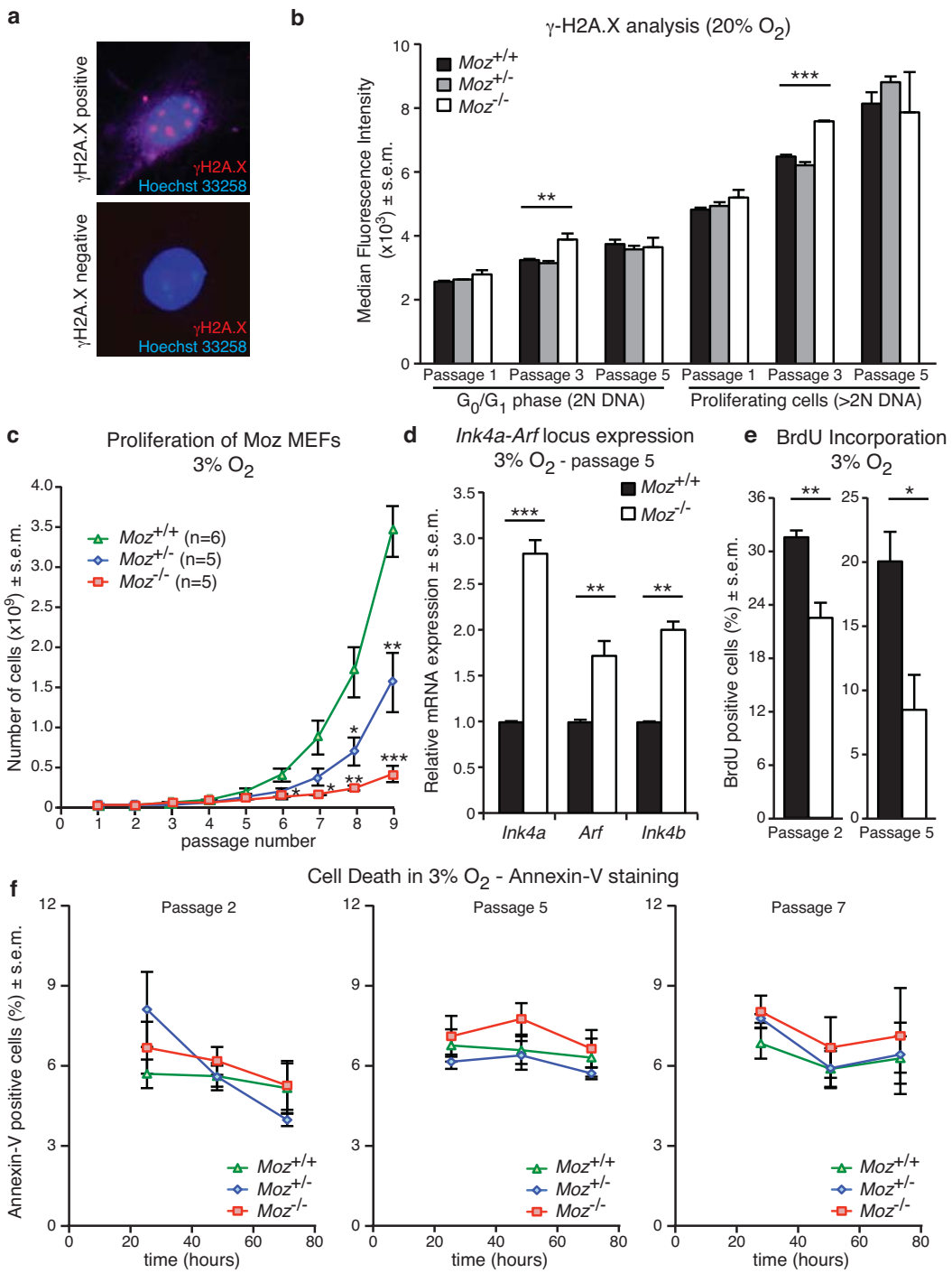
**Figure 6** – H3K9 acetylation is reduced in *Moz*<sup>-/-</sup> MEFs at gene loci that repress senescence

(a) H3K9ac levels were reduced at the transcriptional start sites (TSS) of *Cdc6*, *E2f2*, *Ezh2*, and *Melk*, but not *Skp2* in *Moz*<sup>-/-</sup> cultures. The  $\beta$ -2-microglobulin (*B2m*) gene is provided as a positive control, and the *albumin* gene, which is transcriptionally inactive in MEFs, is provided as a negative control. H3K9ac levels of control genes were not changed in *Moz*<sup>-/-</sup> MEFs compared to wild type. (b) H3K9ac levels were unchanged ~500 bp upstream of the TSS, suggesting that changes in H3K9ac levels in the absence of MOZ are specific to the TSS. (c,d) H3K14ac levels were not different between wild type and *Moz*<sup>-/-</sup> MEFs at the TSS (c) or upstream of the TSS (d) at the *Cdc6*, *E2f2*, *Ezh2*, or *Melk* loci.

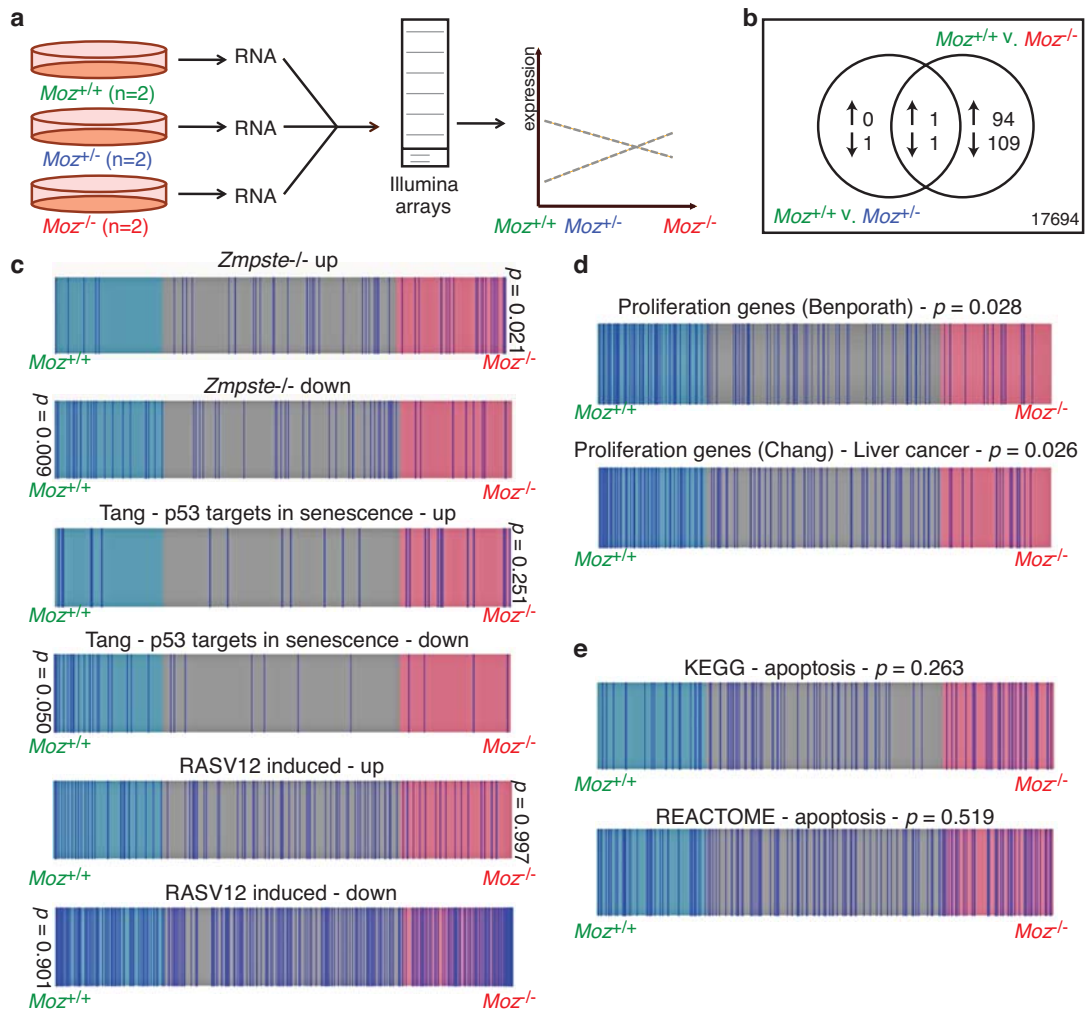
All analyses were carried out on subconfluent MEFs grown in atmospheric oxygen (20% O<sub>2</sub>) at passage 3. H3K9ac levels were standardised to H3K9ac levels at the TSS of the housekeeping gene *Hsp90ab1*, while H3K14ac levels were standardised to H3K14ac at *Hsp90ab1*. n = 3 independent cultures of each genotype. Asterisks mark statistically significant differences between wild type and *Moz*<sup>-/-</sup> cultures at \**p* < 0.05, \*\**p* < 0.01, \*\*\* *p* < 0.001.



Sheikh Figure 1



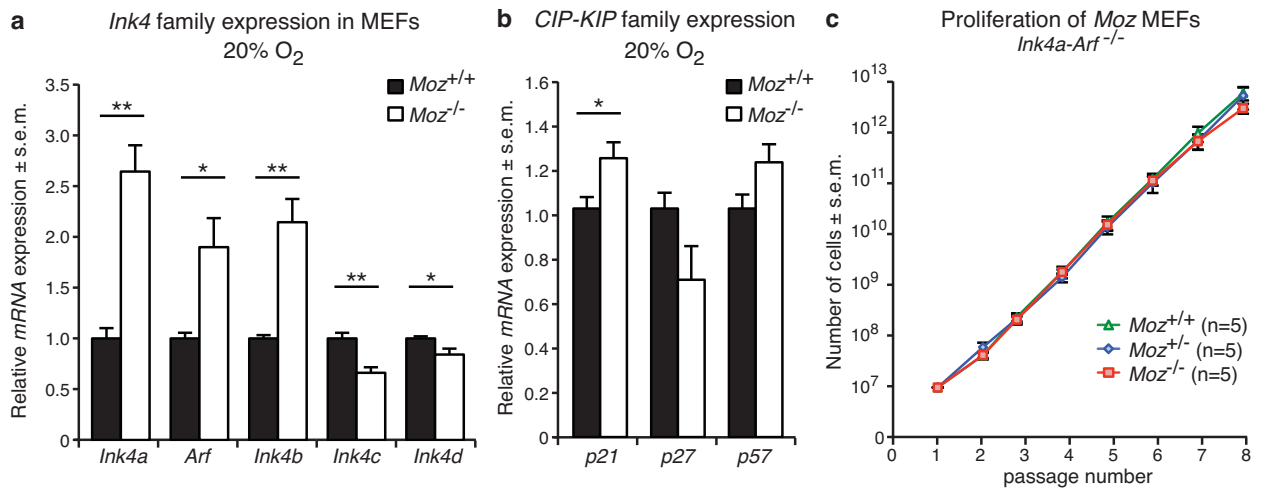
Sheikh Figure 2



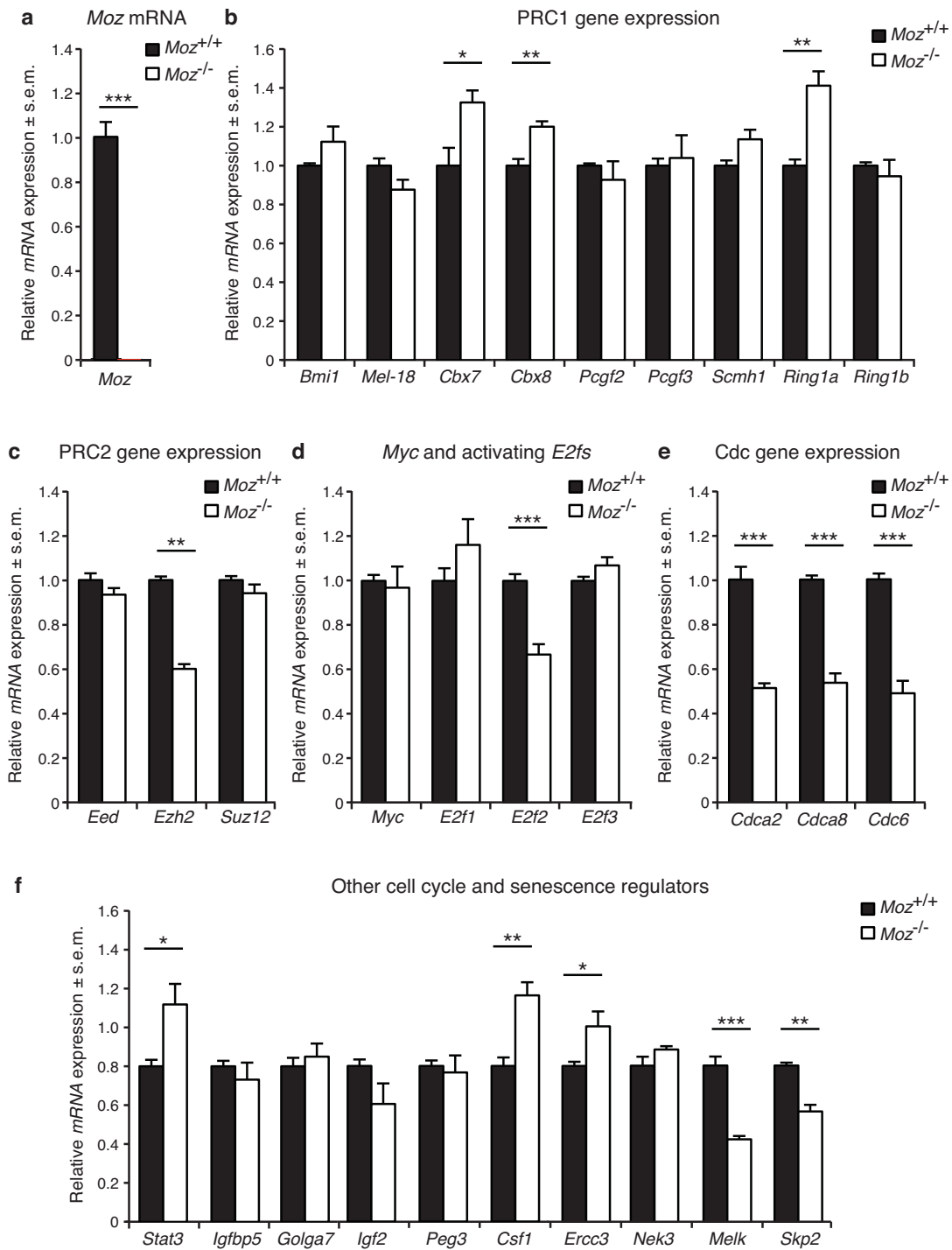
**f**

| Study  | N (genes) | Direction | p value |
|--|-----------|-----------|---------|
| EGUCHI_CELL_CYCLE_RB1_TARGETS                          | 21        | Down      | 0.0130  |
| TARTE_PLASMA_CELL_VS_PLASMABLAST_UP                    | 329       | Up        | 0.0142  |
| VECCHI_GASTRIC_CANCER_EARLY_UP                         | 434       | Down      | 0.0149  |
| NIKOLSKY_BREAST_CANCER_21Q22_AMPLICON                  | 16        | Down      | 0.0162  |
| BENPORATH_ES_CORE_NINE_CORRELATED                      | 138       | Down      | 0.0164  |
| HONRADO_BREAST_CANCER_BRCA1_VS_BRCA2                   | 29        | Down      | 0.0184  |
| GARGALOVIC_RESPONSE_TO_OXIDIZED_PHOSPHOLIPIDS_TURQUOIK | 62        | Down      | 0.0198  |
| REACTOME_ACTIVATION_OF_THE_PRE_REPLICATIVE_COMPLEX     | 30        | Down      | 0.0209  |
| SONG_TARGETS_OF_IE86_CMV_PROTEIN                       | 65        | Down      | 0.0210  |
| BIOCARTA_MCM_PATHWAY                                   | 19        | Down      | 0.0210  |
| SMID_BREAST_CANCER_RELAPSE_IN_BRAIN_UP                 | 44        | Down      | 0.0223  |
| REACTOME_UNWINDING_OF_DNA                              | 18        | Down      | 0.0225  |
| RHEIN_ALL_GLUCOCORTICOID_THERAPY_DN                    | 481       | Down      | 0.0229  |
| RUTELLA_RESPONSE_TO_HGF_UP                             | 444       | Up        | 0.0230  |
| FRASOR_RESPONSE_TO_SERM_OR_FULVESTRANT_DN              | 57        | Down      | 0.0236  |
| RICKMAN_TUMOR_DIFFERENTIATED_WELL_VS_POORLY_UP         | 291       | Down      | 0.0253  |
| KOBAYASHI_EGFR_SIGNALING_24HR_UP                       | 95        | Up        | 0.0254  |
| MARKEY_RB1_CHRONIC_LOF_UP                              | 156       | Down      | 0.0279  |
| PYEON_CANCER_HEAD_AND_NECK_VS_CERVICAL_UP              | 186       | Down      | 0.0297  |
| REN_ALVEOLAR_RHABDOMYOSARCOMA_DN                       | 632       | Up        | 0.0303  |
| HASINA_NOL7_TARGETS_DN                                 | 20        | Down      | 0.0304  |
| HUMMEL_BURKITTIS_LYMPHOMA_UP                           | 42        | Down      | 0.0317  |
| STEIN_ESRRA_TARGETS_RESPONSIVE_TO_ESTROGEN_DN          | 66        | Down      | 0.0333  |
| LY_AGING_PREMATURE_DN                                  | 29        | Down      | 0.0333  |
| SUNG_METASTASIS_STROMA_DN                              | 57        | Down      | 0.0334  |
| REACTOME_CELL_CYCLE_CHECKPOINTS                        | 164       | Down      | 0.0339  |
| LI_WILMS_TUMOR_VS_FETAL_KIDNEY_1_DN                    | 212       | Down      | 0.0340  |
| PUJANA_BREAST_CANCER_WITH_BRCA1_MUTATED_UP             | 77        | Down      | 0.0343  |
| LY_AGING_OLD_UP  | 11        | Up        | 0.0347  |
| LY_AGING_OLD_DN  | 68        | Down      | 0.0353  |

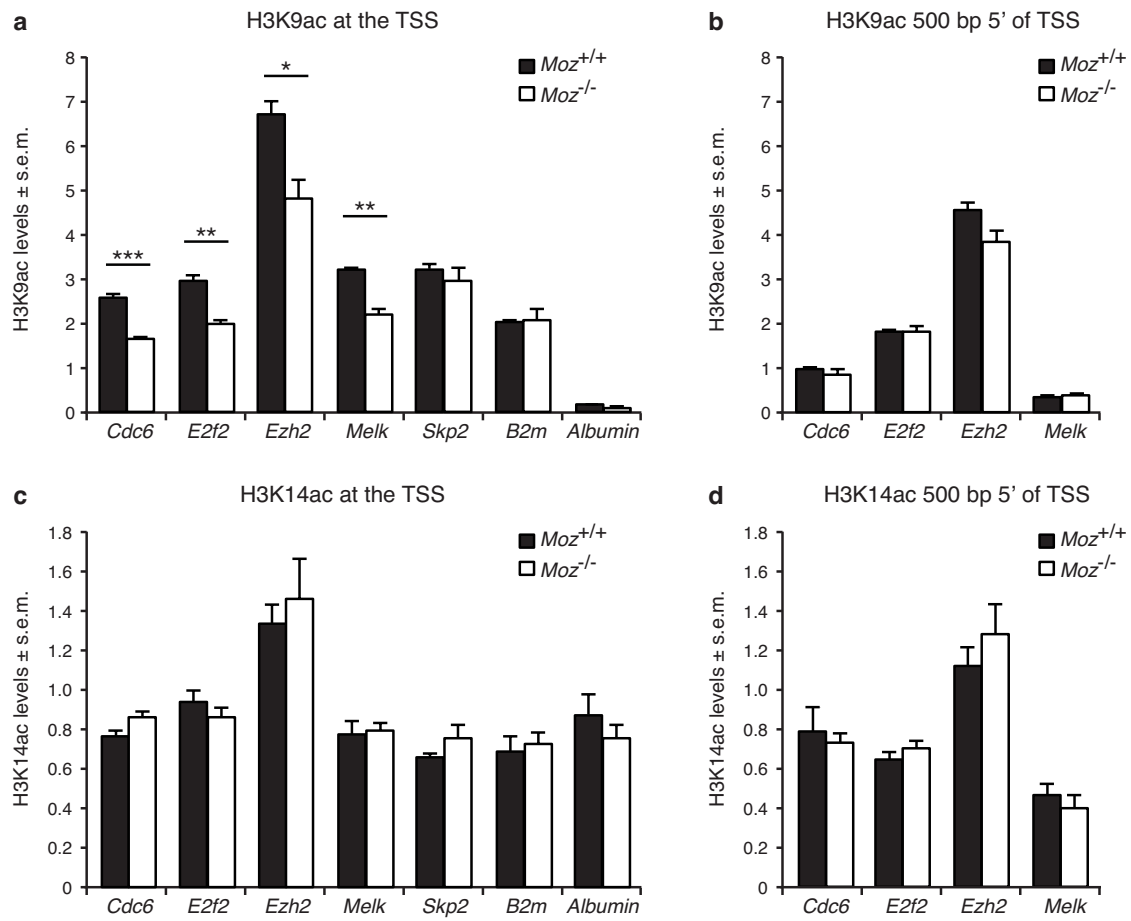
Sheikh Figure 3



Sheikh Figure 4



Sheikh Figure 5



Sheikh Figure 6